Proceedings of the 28th IEEE
EMBS Annual International Conference
New York City, USA, Aug 30-Sept 3, 2006

Segmentation of Lung Lobes in Volumetric CT images for Surgical Planning of Treating Lung Cancer

Q. Wei[1], *Student Member, IEEE,* Y. Hu[1], *Member, IEEE,* J. H. MacGregor[2], and G. Gelfand[2]

[1]Dept. of Electrical and Computer Engineering, University of Calgary, Calgary, AB, Canada
qwei@ucalgary.ca; huy@ucalgary.ca
[2]Foothills Medical Center, Calgary, AB, Canada
macgrejh@shaw.ca; gelfand@ucalgary.ca

***Abstract* - Study has shown that three-dimensional (3D) visualization of lung cavities has distinct advantages over traditional computed tomographic (CT) images for surgical planning. A crucial step for achieving 3D visualization of lung cavities is the segmentation of lung lobes by identifying lobar fissures in volumetric CT images. Current segmentation algorithms for lung lobes rely on manually placed markers to identify the fissures. This paper presents an autonomous algorithm that effectively segments the lung lobes without user intervention. This algorithm applies a two-stage approach: (a) adaptive fissure sweeping to coarsely define fissure regions of lobar fissures; and (b) watershed transform to refine the location and curvature of fissures within the fissure regions. We have tested this algorithm on 4 CT data sets. Comparing with visual inspection, the algorithm provides an accuracy of 85.5 – 95.0% and 88.2 – 92.3% for lobar fissures in the left and right lungs, respectively. This work proves the feasibility of developing an automatic algorithm for segmenting lung lobes.**

***Keywords* - segmentation, lung lobar fissures, visualization.**

I. Introduction

LUNG cancer is the leading cause of cancer death for both men and women in North America [1]. Surgical removal of the diseased lung lobes is the preferred choice for treating lung cancer. In current clinical settings, surgeons / radiologists read two-dimensional (2D) computed tomographic (CT) images of lung cavities for surgical planning. These CT images offer 2D view from one viewpoint and in different shades of gray; therefore reading them is a highly subjective task and requires strenuous mental work to map anatomic structures from stacks of 2D images onto actual lung cavities in three dimensions. This leads to a heavy workload, long planning time, and low accuracy in the predicted surgical removal of lung cancer.

Current standard CT scanners produce images with a slice thickness of 5.0 mm. A complete scan of an average person's lung cavity requires approximately 60 images. Advanced multi-slice CT scanners are capable of producing images with a slice thickness of 0.1 – 0.6 mm. As a result, surgeons need to read over 500 images for the same lung cavity. This sheer number of CT images exceeds the human ability for handling information. An efficient surgical planning system is needed to alleviate this situation.

With the emergence of virtual reality technologies, three-dimensional (3D) visualization of anatomic structures is gaining popularity in surgical planning [2, 3]. Unlike conventional 2D views, 3D visualization provides multi-viewpoints, colors, stereoscopic view, and no need for mental reconstruction. Fig. 1 illustrates the differences between the 2D view of conventional CT images and 3D visualization of lung cavities reconstructed from a stack of 2D CT images by manually segmenting lung lobes. Our recent study has revealed that 3D visualization of lung cavities has distinctive advantages over conventional CT images for surgical planning [4]. The foremost challenge for 3D visualization of lung cavities is the ability to automatically segment lung lobes from a stack of CT images, so that the use of the 3D visualization would be practical in clinical settings for surgical planning.

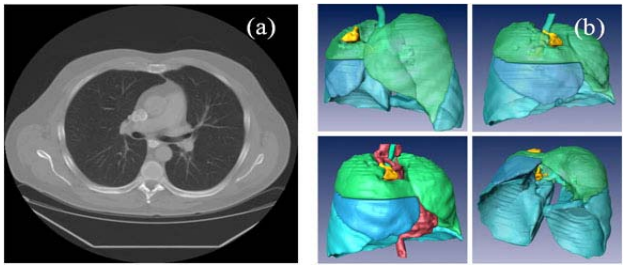

Fig. 1.Difference between the 2D view of conventional CT images (a) and 3D visualization of lung cavities reconstructed from a stack of 2D CT images by manually segmenting lung lobes (b).

To meet this challenge, several research groups have developed various algorithms to segment lung lobes. Kuhnigk and colleagues [5], as well as Ukil and colleagues [6], have developed algorithms for segmenting lung lobes based on the approach of combining 3D watershed transform and anatomic information of a segmented airway tree. This approach works well for lobar fissures in both high and low contrast, provided that no vessels cross from one lobe to another and adequate markers are placed to guide the algorithm. Zhang and colleagues [7-9] have taken another approach to segment lung lobes using fuzzy reasoning, 3D shape constraints, and an atlas with a priori knowledge. Their algorithm produces accurate results under the condition that lobar fissures are always in high contrast

and the user provides sufficient markers and training data. All of these algorithms have relied on manually placed markers to reliably segment the lung lobes.

Without the placement of markers, we have developed an autonomous segmentation algorithm to effectively identify lobar fissures. This algorithm takes a two-stage approach to process stacks of CT images. In the first stage, we use adaptive fissure sweeping to automatically find the regions of lobar fissures based on general lung anatomy. In the second stage, we apply watershed transform to refine the location and curvature of these fissures. We present our algorithm in this paper with the following structure of contents. Section II is a brief introduction to the anatomy of the lungs. In Section III, we describe our two-stage approach of segmentation, followed by the results of the segmentation and discussions in Section IV. Finally, we present our conclusion and future work.

II. Lung Anatomy

Fig. 2 shows the general anatomic structure of human lungs, which have five distinct partitions called lobes. The boundaries of the lobes are lobar fissures. The right lung usually consists of 3 lobes: the superior, middle, and inferior lobes. The right oblique fissure separates the superior and middle lobes, while the horizontal fissure separates the middle and inferior lobes. The left lung usually consists of 2 lobes: the superior and inferior lobes, which have a boundary of the left oblique fissure. In general, the lobes function relatively independent of each other, with no major airways or vessels crossing the lobar fissures.

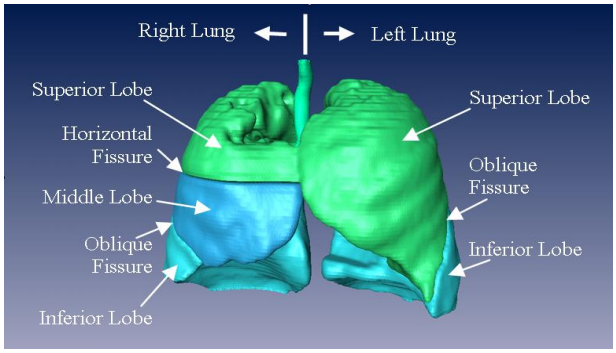

Fig. 2. The general anatomy of human lungs.

III. Methodology

Using knowledge from the general lung anatomy, our algorithm (written in Matlab) takes a two-stage approach to find the lobar fissures in the left and right lungs. Given the CT images where fissures are present, the algorithm first uses adaptive fissure sweeping to define the region of the fissures. The algorithm then uses watershed transform to refine the fissure location and curvature from the found fissure regions in the first stage. Fig. 3 shows the flow diagram of this segmentation algorithm. We describe these two stages in the following two sub-sections, separately.

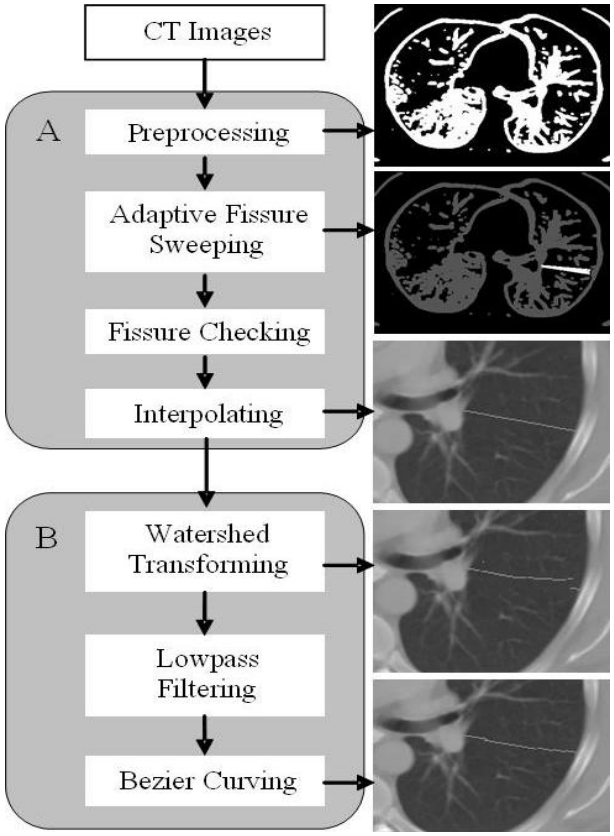

Fig. 3. Flow diagram of the segmentation algorithm showing the two-stages approach: adaptive fissure sweeping (A) and watershed transform (B). The right column of the diagram shows the corresponding processed images for the algorithm.

A. Adaptive Fissure Sweeping

In this stage, the first step is to use a thresholding technique for extracting the rib cage and lung boundaries. For each patient, a threshold value is determined based on the mean pixel intensity value of the CT images. A region of interest containing the lungs is defined within the rib cage. This eliminates the processing of anatomic structures outside the lungs. The lung atlas is then applied based on the size of the lungs found from the lung boundaries.

The second step is to preprocess all CT images. The airway tree and vessels are first extracted by using the thresholding technique. Once again, the threshold value is selected based on the mean pixel intensity value of the CT images. The median filter is then applied to reduce noise left from thresholding. Then the airway trees and vessels are enhanced (widened) using vessel weighting (larger vessels are given higher pixel intensity values) and Gaussian blurring. This treatment produces binary images, in which a pixel represents either air or airway tree/vessels in the lungs.

From the general anatomic structure of the lungs as shown in Fig. 2, the lobar fissures separate the lung lobes where no major airways or vessels cross. This means that in the preprocessed binary images, fissures are represented by large amounts of air or space extending from the middle of the lungs to the lateral side of the lungs. Our technique of

adaptive fissure sweeping takes advantage of this information to coarsely define empty regions where fissures could be present. The technique uses various predefined fissure angles (defined by angles between the fissures and a flat horizontal line) defined from the lung atlas. At each angle, the technique sweeps a number of fissures across the lung and then automatically checks the sweeping results to determine the most probable fissure angle and location using statistical analysis. An evaluation variable is calculated from a number of parameters. The likelihood of the fissure region that is correct at the current angle compared to a previous angle is defined by

$$P = W_1(\Delta\sigma_{x,y}) + W_2(\Delta\sigma_r) + W_3(\Delta N) + W_4(\Delta R) + W_5(\Delta\Phi),$$

where Δ represents change in parameters – $\sigma_{x,y}$, σ_r, N, R, and Φ – between two consecutive sweeping angles [$\sigma_{x,y}$ is the standard deviation of fissures within a fissure region in x and y coordinates; σ_r is the standard deviation of the fissure length; N represents the number of the fissures swept; R is the average length of the fissures; and Φ is the change of angle between the swept angles and the angle of the fissures found in the previous CT slice]. The weights W_1, W_2, W_3, W_4, and W_5 have different values assigned to the corresponding parameters from one region to another in the lungs, because fissures have distinctive characteristics for each region (*e.g.* length and change in angles between two adjacent CT slices, etc.). Generally, high weights emphasize characteristics in a region whereas low weights deemphasize. For each fissure angle, the above equation yields a P value. We select the angle with the highest P value as the correct fissure angle to define the fissure region.

In addition, the technique of adaptive fissure sweeping checks for fissure smoothness in 3D. As shown in Fig. 2, lobar fissures flow smoothly in 3D from the top to the bottom of a lung. Thus, the technique automatically rejects a probable fissure, which causes an abrupt change in fissure locations between two adjacent CT slices.

To fill in the space of a rejected fissure, the technique of adaptive fissure sweeping performs a linear interpolation by using four endpoints of two known fissures to estimate the current location of a probable fissure, provided these known fissures are only a few slices apart. The technique also extends fissures which do not extend to the edges of the lung or vessels by using the lung boundaries extracted earlier.

B. Watershed Transform

In the second stage of our algorithm, we use the technique of watershed transform on the original CT images to refine the fissure location and curvature within the fissure regions found in the first stage of the algorithm. Unlike conventional watershed transform where watershed or local maxima are found, the technique searches for minima that represent the location of the fissures. First, to remove some of noise and pixel non-uniformity without over blurring the image, we generate a Gaussian filter kernel of 10 x 10 pixels, because the fissure region is approximately 10 pixels wide. As a result, this filter prevents the issue of over-segmentation that conventional watershed transform produces. Then, we apply the watershed transform within the region of the fissure found in the first stage. In the blurred images, the technique refines the true fissure curvature and location by using the minima found in the fissure region.

In many cases, the minima found within the fissure region may not be smooth, because of pixel non-uniformity and noise presented in the CT images. We utilize a 5^{th}-order Butterworth lowpass filter (for balancing between a sharp roll-off and computational load) to remove high frequency noise in the fissure and the Bezier curving method [10] to further smooth the fissure. Maxima and minima of the low frequency noise in the fissure are used as control points for Bezier curving to yield a fissure with a smooth curvature.

IV. Results and Discussions

To test the algorithm, we processed CT images from 6 anonymous patients from London Health Sciences Center, London, ON. Four of the 6 patients had tumors present in the left or right lung, which disrupted lobar fissures. For these patients, we only used the side of the lungs where no predominate tumors were present and fissures were intact to test the suitability of our algorithm. The other two patients had no tumors that affected the lobar fissures, so we used both their left and right lungs in the test. This allowed us to test our segmentation algorithm on four CT data sets for the left and right lungs, respectively.

All CT images have a resolution of 512 x 512 pixels with a thickness of 2.5 ~ 7.0 mm. Fig. 4 shows the results of left and right lung segmentation from the CT images of two patients, who had no predominate tumors to disrupt lobar fissures. In addition, Fig. 4 compares the fissure found from our algorithm (represented by white lines in e and f) and the fissure traced by a radiologist (represented by arrows and a circle in g and h, showing locations of the oblique fissures and the region of the horizontal fissure respectively). As illustrated in Fig. 4, the results of the algorithm are very close to that indicated by the radiologist.

Table I and Table II describe the accuracy and performance of the algorithm for segmenting the left and right lungs respectively. To determine the accuracy of the algorithm, we compared the visually inspected location of the fissures to that of the fissures found by the algorithm. We obtained an accuracy of 85.5 – 95.0 %, 88.2 – 92.3% and 100 % for segmenting the left oblique, the right oblique, and the right horizontal fissures respectively. We evaluated the performance of our algorithm using a 2.8 GHz Pentium 4 computer with 1 GB of RAM running Matlab 7.0.4 (R14). All segmentations (on the left or right lung) were processed under two minutes.

Although our algorithm produces results in good agreement with what a radiologist has identified, there are small variations in the accuracy yielded by our algorithm in segmenting the left and right oblique fissures, as described

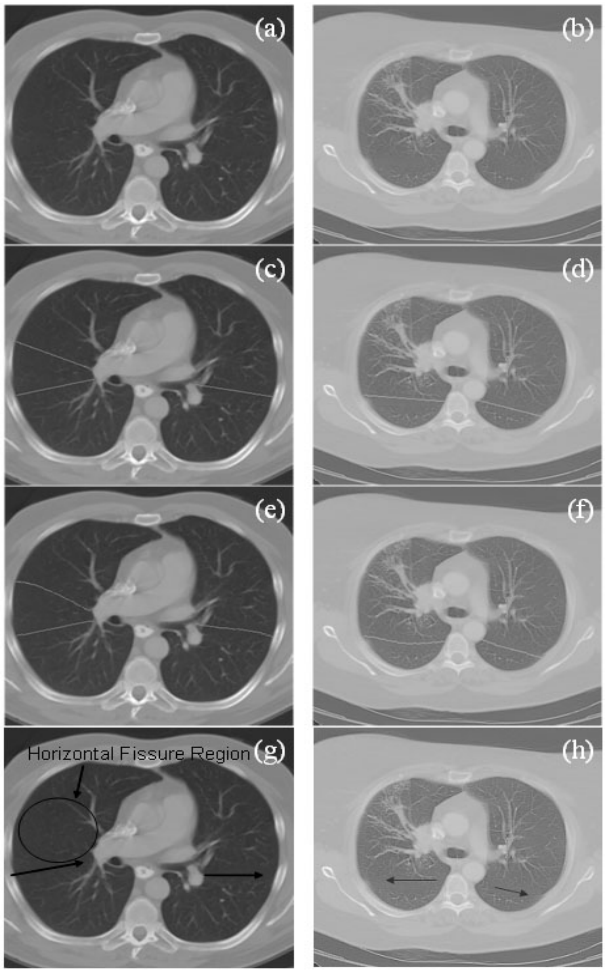

Fig. 4. Sample segmentation results from patient A (left column) and patient B (right column). (a) (b) The original CT images. (c) (d) The processed CT images showing found fissure region using adaptive fissure sweeping. (e) (f) The final fissure with curvature refined by watershed transform. (g) (h) The fissure regions marked manually by a radiologist [The arrows represent the location of the oblique fissures while the circle in (g) shows the region of the horizontal fissure].

TABLE I
PERFORMANCE AND ACCURACY FOR SEGMENTING THE LEFT LUNG

Patient	Slice Thickness (mm)	Number of Slices Processed	Left Lobar Fissure Accuracy (%)		Run Time (m:s)
			Oblique Fissure	Horizontal Fissure	
#1	3.5	40	95.0	-	1:33
#2	3.5	36	88.9	-	1:06
#3	2.5	55	85.5	-	1:58
#4	3.5	39	89.7	-	1:12

TABLE II
PERFORMANCE AND ACCURACY FOR SEGMENTING THE RIGHT LUNG

Patient	Slice Thickness (mm)	Number of Slices Processed	Right Lobar Fissures Accuracy (%)		Run Time (m:s)
			Oblique Fissure	Horizontal Fissure	
#1	3.5	40	90.9	100	1:50
#2	3.5	36	92.3	100	1:51
#5	7.0	11	90.9	100	1:10
#6	7.0	17	88.2	100	1:18

in Table I and Table II. This is mainly due to anatomic variations among human lungs from one individual to another. For example, the left lung segmentation of Patient #3 shows the lowest accuracy since the lung varied the most from the rest of test data sets. In these test data sets, the fissure angles change gradually as the fissure moves from the top towards the bottom of the lung, as illustrated in Fig. 2. The fissure angles of Patient #3, in contrast, remain mostly constant and, consequently, might contribute to a slightly higher error rate. In general, thinner CT slices yield higher accuracy, because more information is available. We anticipate that testing the algorithm on 0.6 mm CT images would yield more accurate segmentation results.

V. CONCLUSION AND FUTURE WORK

In conclusion, we have developed an autonomous algorithm for segmenting the lung lobes. Using the techniques of adaptive fissure sweeping and watershed transform, the two-stage algorithm provided an accuracy of 85.5 – 95.0% and 88.2 – 92.3 % for segmenting lobar fissures of the left and right lungs, respectively. This result promises a potential to develop an automatic algorithm with higher accuracy in segmenting lung lobes for the 3D surgical planning of treating lung cancer. Future work includes: (1) evaluating our algorithm using a large variety of patient data and thinner CT images; and (2) porting the final algorithm from Matlab into C to improve performance.

REFERENCES

[1] American Cancer Society, "Cancer Facts & Figures," [Online], 2006, Available at: http://www.cancer.org/docroot/STT/stt_0.asp

[2] S.J. Wigmore, D.N. Redhead, et al., "Virtual hepatic resection using three-dimensional reconstruction of helical computed tomography angioportograms," *Ann. Surg.*, vol. 233, pp. 221-226, 2001.

[3] S.W. Lee, H. Shinohara, et al, "Preoperative simulation of vascular anatomy by three-dimensional computed tomography imaging in laparoscopic gastric cancer surgery," *J. Ameri. Colleg. Surg.*, vol. 197, pp. 927-936, 2003.

[4] Y. Hu, "The role of three-dimensional visualization in surgical planning of treating lung cancer," in *27th Annu. Intl. Conf. IEEE EMBC*, Shanghai, China, 2005.

[5] J.-M. Kuhnigk, H. K. Hahn, et.al, "Lung lobe segmentation by anatomy-guided 3-D watershed transform," *Proc. SPIE (Med. Imag.)*, vol. 5032, pp. 1482–1490, 2003.

[6] S. Ukil, E. A. Hoffman, and J. M. Reinhardt, "Automatic lung lobes segmentation in X-ray CT images by 3D watershed transform using anatomic information from the segmented airway tree," *Proc. SPIE (Med. Imag.)*, vol. 5747, pp. 556–567, 2005.

[7] L. Zhang and J. M. Reinhardt, "Detection of lung lobar fissures using fuzzy logic," *Proc. SPIE (Med. Imag.)*, vol. 3660, pp. 188–199, 1999.

[8] L. Zhang, E. A. Hoffman, and J. M. Reinhardt, "Lung lobe segmentation by graph search with 3-D shape constraints," in *Proc. SPIE (Med. Imag.)*, vol. 4321, pp. 204–215, 2001.

[9] L. Zhang, E. A. Hoffman, and J. M. Reinhardt, "Atlas-driven lung lobe segmentation in volumetric x-ray CT images," *IEEE Trans. Med. Imag.,* vol. 25, pp. 1-16, 2006.

[10] P. E. Bezier, *Employ des Machines á Commande Numérique*, Mason et Cie, Paris, 1970. Translated by Forrest, A. R., and A.F. Pankhurst as P. Bézier, *Numerical Control– Mathematics and Applications*, Wiley, London, 1972.